JOURNAL OF MATERIALS SCIENCE 20 (1985) 2110–2118

Thermal evolution and mechanical properties of vitreous fibres in the SiO_2–Li_2O–TiO_2–Al_2O_3 system

G. SORARU
Istituto di Chimica Industriale dell'Università di Padova, Via Marzolo 9, 35100 Padova, Italy

G. FAGHERAZZI, M. BOTTARELLI, A. BENEDETTI
Dipartimento di Spettroscopia, Elettrochimica e Chimica Fisica dell'Università di Venezia, Calle Larga S. Marta DD 2137, 30123 Venezia, Italy

The thermal evolution of glass fibres of the SiO_2–Li_2O–TiO_2–Al_2O_3 system has been investigated by X-ray diffraction, DTA and SEM. Within the range of the compositions investigated (2 to 10 mol % TiO_2) SEM and SAXS measurements on bulk materials have shown that a small addition of Al_2O_3 (3 mol %) does not modify the limits of the immiscibility region present in the ternary system SiO_2–Li_2O–TiO_2. Within this region TiO_2-rich droplets are more than likely to be formed. As to tensile strength, the "as-quenched" fibres of the composition placed within the immiscibility dome give higher values than that obtained outside the liquid–liquid region and these values are higher than those measured on E-glass fibres. A slight crystallization in all the fibres leads to a continuous decrease of the initial tensile strength. With regards to the crystal phases presented by the crystallized fibres, the first exothermic peak is due to the simultaneous crystallization of β-quartz (ss) and lithium disilicate whereas the second peak is due, most probably, to a β-quartz (ss) → β-spodumene (ss) phase transformation as well as to the formation of Li_2TiSiO_5. The path of crystallization of the other detected Ti-compounds is similar to that proposed by Furukawa and White.

1. Introduction

In recent years, the preparation of lithium-bearing glassy and glass–ceramic materials, involving the formation of crystalline species of low thermal expansion, have become increasingly important. The SiO_2–Li_2O–TiO_2–Al_2O_3 system belongs to this class of glasses of technological relevance having a wide glass-forming composition range. The fact that the fibres can be drawn [1–3] has further increased the application range of these glasses. So far, the possibility to improve the mechanical properties of vitreous fibres through a controlled microstructure obtained by heat treatments is an open question. The results reported in the literature [1, 4, 5] about the mechanical properties of glass–ceramic fibres suggest that the main controlling factors of the tensile strength are crystallinity, the crystallite dimensions, the crystal preferred orientation and the more or less homogeneous dispersion of the phases formed. For these reasons, a detailed knowledge of the thermal evolution of the glassy systems is necessary in order to deepen the knowledge of the relationships between microstructure and mechanical properties of the derived glass–ceramic materials.

In the present work, which is a part of a more comprehensive research programme [2, 3, 6–9], the crystallization process of glass fibres of three different compositions in the system SiO_2–Li_2O–TiO_2–Al_2O_3 will be discussed. The ternary phase diagram SiO_2–TiO_2–Li_2O has been investigated

0022–2461/85 $03.00 + .12

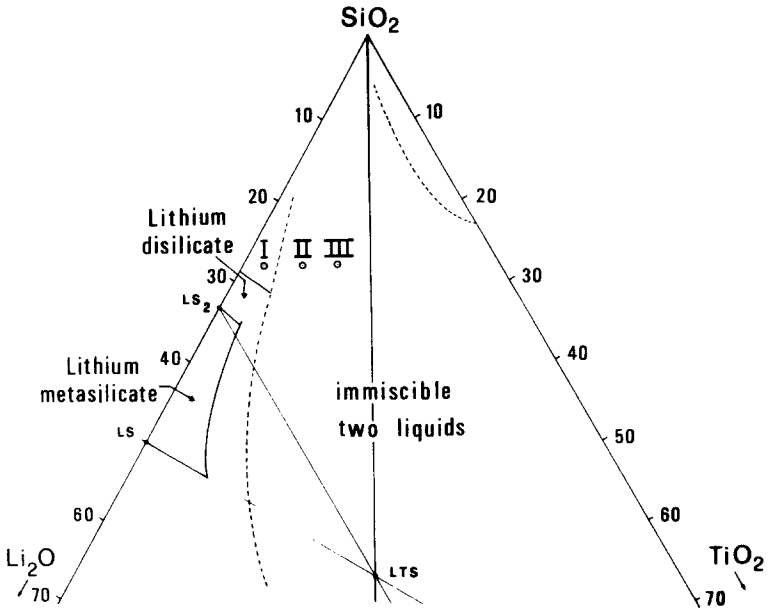

Figure 1 Ternary phase diagram Li_2O–SiO_2–TiO_2 (mol%) [11]. LS = Lithium metasilicate, LS_2 = Lithium disilicate, and LTS = Li_2TiSiO_5.

by Fields *et al.* [10] in order to study the possibility of strengthening the glass by an amorphous phase separation. Apart from a constant, small amount (3 mol%) of alumina, we have examined compositions similar to those studied by Fields *et al.*, by starting with a single glassy phase and gradually moving into the immiscibility region. Also the influence of glass-in-glass phase separation on the subsequent crystallization process and on a possible crystal preferred orientation, has been examined.

The thermal evolution of the initial vitreous fibres towards fibres having a glass–ceramic microstructure has been followed by differential thermal analysis (DTA) and wide-angle X-ray diffraction (XRD). To investigate the microstructural features of the materials, SEM and optical microscopy have been used. In order to confirm the SEM results, glass-in-glass phase separation has also been directly studied by small-angle X-ray scattering (SAXS).

Finally, preliminary results about fibre tensile strength dependence on heat treatment have been reported.

2. Experimental section and methods

Fibres with a mean diameter of 10 to 15 μm have been drawn from the melt at temperatures ranging between 1160 and 1230° C using an experimental apparatus described elsewhere [2]. Three glass compositions (called I, II and III) have been investigated (see the ternary diagram of Fig. 1, in which alumina has been excluded, and Table I). A fourth composition, having the same SiO_2, Li_2O and TiO_2 relative contents of composition III, but without alumina, has also been investigated in a massive sample for comparative purposes.

2.1. Optical and electronic microscopies

As-quenched and partially crystallized fibres were checked under a polarizing microscope (Leitz). SEM (Cambridge) investigations were carried out on both crystallized fibres and freshly fractured surfaces of the corresponding bulk samples. A slight etch with a 2% HF solution for periods of time ranging between 15 sec and 1 min were performed on the same samples before SEM examinations.

2.2. DTA analysis

To perform differential thermal analysis on powdered glass fibres a Netzsch apparatus with calcined alumina as the reference material was used. The following experimental conditions

TABLE I Chemical composition in mol% of the glassy systems (wt% within parentheses)

Oxide	Glassy systems			
	I	II	III	IV
SiO_2	70 (77.8)	70 (75.0)	70 (72.4)	72.2 (76.4)
Li_2O	25 (13.7)	21 (11.1)	17 (8.7)	17.5 (9.2)
TiO_2	2 (2.9)	6 (8.5)	10 (13.6)	10.3 (14.4)
Al_2O_3	3 (5.6)	3 (5.4)	3 (5.2)	–

were set: heating rate of 10° C min^{-1}; sensitivity of 0.1 mV for a full scale expansion; sample weight of 200 mg.

2.3. Tensile and test procedure

A fibre was glued with a polyester resin on two cardboard supports and then mounted in the grips of the testing machine. All tests were carried out in the laboratory atmosphere using an Instron testing machine on 25 mm gauge length specimens with a strain rate of 10 min^{-1}. Fibre diameters were measured before and after the strength experiments by optical microscopy with a scale inside the ocular lens. The precision was $\simeq \pm 0.4$ μm. The The accuracy of the tensile strength measurements was $\simeq 3.5\%$.

With regards to a heat treatment preceding the tensile tests, the fibres were laid out between two refractory supports and thus introduced into the furnace. The tensile tests were performed on the part of the fibres which did not touch the refractory materials. Every strength measurement was averaged at least on ten heat-treated fibres.

2.4. Wide-angle X-ray diffraction (XRD)

A Philips vertical diffractometer, equipped with Soller slits, a graphite focusing crystal as monochromator and a scintillation counter supplied with a pulse height analyser were used. The X-ray diagrams (Cu$K\alpha$ radiation) were recorded with a goniometer scanning rate of 0.25° min^{-1} and a RC time constant of 4 sec.

2.5. Small angle X-ray scattering (SAXS)

SAXS measurements were carried out according to "infinite primary beam" conditions with a Kratky–Paar camera equipped with an electronic step-scanner. Zirconium-filtered Mo$K\alpha$ with pulse height discriminator and a proportional counter were employed. SAXS intensities, averaged over several runs to accumulate 10^5 counts per point, were recorded. The analysis was carried out on an "as-quenched" platelet of composition III.

The volume distribution function $d_v(R)$ of the size of spherically shaped particles was deduced using a Titchmarsh transform of the scattered slit smeared intensity $J(h)$, where $h = 4(\sin\theta)/\lambda$ where 2θ is the diffraction angle and λ is the wavelength of the radiation employed [12], as follows:

$$d_v(R) \propto R \int_0^\infty [h^3 J(h) - K] \times [2J_0(hR) + J_1(hR)(hR - 3/hR)]\,dh$$

$K = \lim_{h\to\infty} h^3 J(h)$ is the Porod asymptotic constant, J_0 and J_1 are zero and first order Bessel functions, respectively.

3. Results and discussion

3.1. Phase separation on the "as-quenched" glasses

The investigation of the "as-quenched" fibres carried out by both optical microscopy and SEM shows the regularity of the diameters and the absence of air bubbles as well as of the other defects either on the surface or inside the samples (Fig. 2). By using SEM and SAXS analyses, performed on glass platelets, we verified that the presence of Al_2O_3 does not modify the limits of the miscibility gap presented in the SiO_2–Li_2O–TiO_2 system as reported by Fields *et al.*, at least for our compositions. The SEM micrographs of sample I have shown complete homogeneity of this glass, whereas composition II exhibits a very fine texture at the limit of the resolving power of the technique. As regards composition III, Fig. 3 shows a SEM photograph in which a lot of nearly spherical droplets of about 35 nm clearly appear.

On this sample the $d_v(R)$ volumetric particle size distribution has been deduced by SAXS (Fig. 4). From this curve an average value of about 20 nm was obtained which is in fairly good agreement with the SEM data, bearing in mind that SEM data are almost always overestimated with respect to SAXS data. Fig. 5 shows the $h^3J(h)$ against h plot from which it is possible to note the excellence of the constance of the Porod limit whereas the initial broad peak may be ascribed to the sphericity of the scattering particles [13].

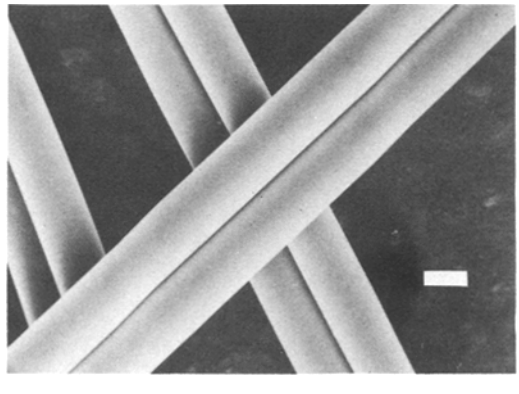

Figure 2 SEM micrograph of fibres III. The bar corresponds to 10 μm.

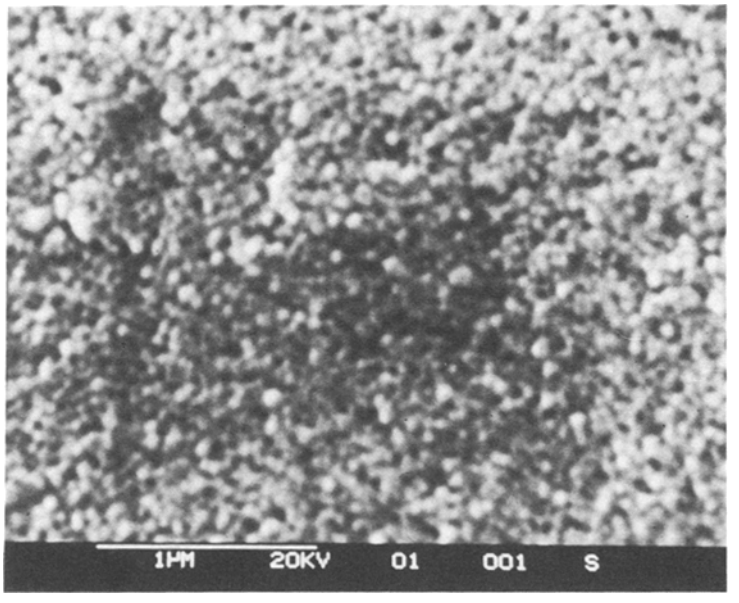

Figure 3 SEM micrograph of a freshly fractured surface of an "as-quenched" bulk sample of composition III. The bar corresponds to 1 μm.

The asymmetry of the $d_v(R)$ curve which is skewed towards the smaller R values indicated that an Ostwald ripening mechanism had taken place in the coarsening process of the demixed phase [14, 15].

Bearing in mind that a SAXS scattering may be detected only if a sufficiently high electron density difference between particles and matrix occurs, it is possible to conclude that our SAXS data qualitatively agree with the hypothesis of Fields *et al.* [10] who suggested that the separate phase was constituted of TiO_2-rich droplets. Also Furukawa and White [16] observed in a SiO_2–Li_2O–TiO_2 system, for a concentration of TiO_2 similar to that of our sample III, the formation of TiO_2-rich droplets. On the other hand, Nakagawa and Izumitani [17] observed the formation of silica-rich droplets in glasses of the same system, but these were richer in TiO_2 (22.5 wt%).

3.2. Thermal evolution of the materials

Fig. 6 shows the DTA curves of fibres I, II and III as well as of a coarse powder of composition IV. A description of the crystallization process inherent to the first exothermic peak (650 to 750° C), due to a simultaneous formation of two phases, i.e. β-quartz solid solution (very similar to β-quartz) and lithium disilicate, was reported in a previous work [3]. In that paper an XRD analysis, carried out *in situ*, at high temperature, was presented, from which it was possible to study the kinetics of the crystallization process.

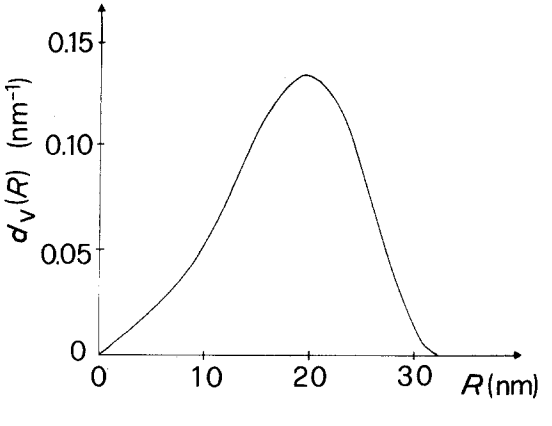

Figure 4 Particle size distribution $d_v(R)$ for an "as-quenched" platelet of composition III obtained by SAXS measurements.

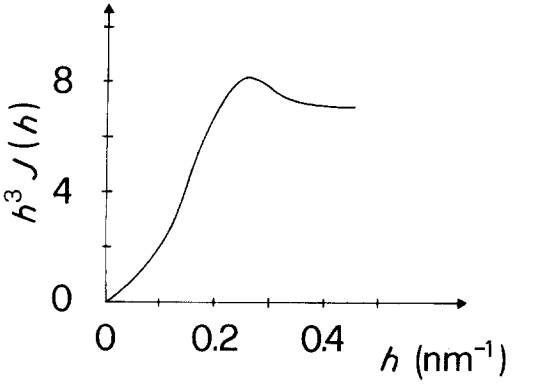

Figure 5 Plot of $h^3 J(h)$ against h for the sample indicated in Fig. 4.

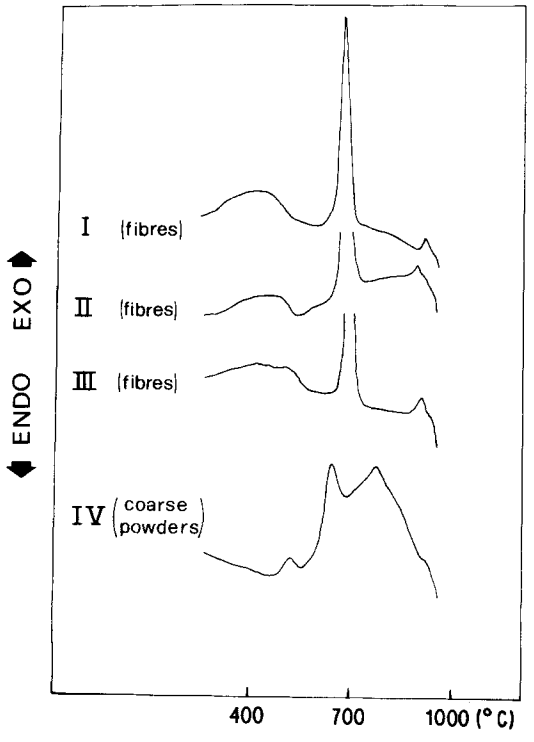

Figure 6 DTA traces for fibres I, II and III and for composition IV.

The morphological indexes, present as exponents in the Avrami equation [18, 19], were computed for the thermally pre-treated specimens, in the range between 1 and 2, thus showing that the contribution of the surface crystallization has to be considered a significant one.

The crystal preferred orientation of the above mentioned two phases which crystallize in correspondence with the first exothermic DTA peak was investigated by using fibre bundles placed inside capillaries of 0.5 mm diameter mounted in a cylindrical X-ray camera of 57.3 mm diameter. While the spectra of fibres II and III do not present orientation effects, the spectrum of fibres I heat treated at 595° C for 2.5 h shows an overintensified equatorial 0 0 2 reflection due to $Li_2Si_2O_5$ (Fig. 7). Bearing in mind that the X-ray beam was perpendicular to the fibre axis, we can conclude that this phase has the *c*-axis of its orthorhombic lattice preferentially lying normal to the external surface and radially placed with respect to the fibre axis. Thus, it was possible to conclude that the absence of a crystal preferred orientation may be favoured by the presence of a glass-in-glass phase separation mechanism preceding the crystallization process.

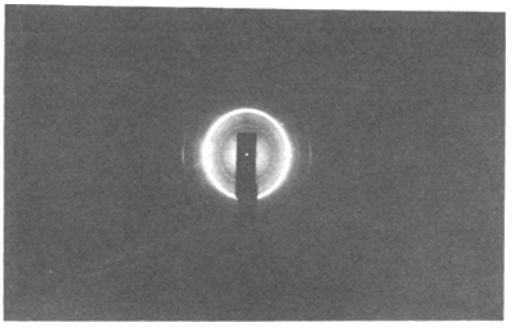

Figure 7 Fibre spectrum of composition I after a heat treatment at 595° C for 2.5 h. The preferred orientation of 0 0 2 reflection clearly appears.

In order to follow the development of the phases related to the 2nd exothermic DTA peak, fibres I, II and III were heated at 800, 850 and 950° C for 2 h and subsequently quenched in air. The first temperature was about in the middle of the two DTA peaks. The second one was placed at the beginning of the 2nd exothermic peak whereas the third temperature was selected beyond this peak. The crystalline phases, determined by XRD and originated by the heat treatments, are reported in Table II. In addition to

TABLE II Phase data of heat treated fibres

Heat treatment	I	II	III
800° C/2 h	D(s), β-q(s) M(m), R(w), β-sp(w)	D(m), β-q(s) M(s), R(w), Ti–X(vw)	D(m), β-q(s) M(m), R(w), Ti–X(m)
850° C/2 h	D(s), β-q(s), M(w) β-sp(m), R(vw) LTS(w)	D(s), β-q(s), M(m) β-sp(vw), R(m) LTS(m)	D(m), β-q(s), M(m) β-sp(w), R(s) LTS(w), Ti–X(vw)
950° C/2 h	D(s), β-sp(s) LTS(m)	D(s), β-q(s) LTS(s), β-sp(s)	D(m), β-q(s) LTS(s), β-sp(m)

Nomenclature: D = Li-disilicate, β-q = β-quartz (ss), M = Li-metasilicate, β-sp = β-spodumene (ss), R = Rutile, LTS = Li_2TiSiO_5, Ti–X = unknown phase.

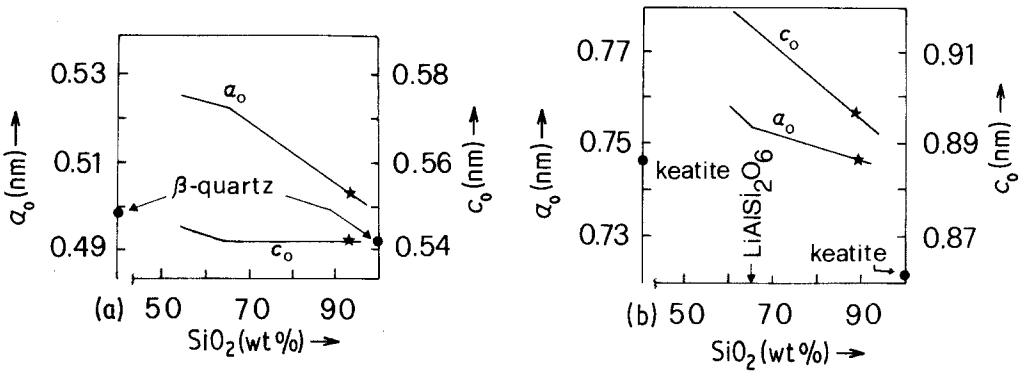

Figure 8 (a) Relationship between lattice parameters of β-quartz (ss) and SiO_2 content in glass [20]. The stars indicate our data. (b) Relationship between lattice parameters of β-spodumene (ss) and SiO_2 content in glass [21]. The stars indicate our data.

β-quartz (ss) and lithium disilicate, all the samples heated at 800° C showed the presence of rutile and lithium metasilicate. An unknown phase, probably containing titanium, here named Ti–X in analogy with that reported by Furukawa and White [16], was present only in compositions II and III which were richer in titanium. This latter compound was found also in the IV glass–ceramic material heated at 820° C. Therefore, we can exclude the presence of aluminium in this phase. The formation of β-spodumene (ss) occurred at a lower temperature for fibres I than for fibres II and III. In all fibres I, II and III we detected at 850° C the ternary phase Li_2TiSiO_5. It is interesting to remark that the appearance of this phase does not lower the X-ray peaks of rutile in compositions II and III. This fact can be explained following the work of Furukawa and White [16]. A part of TiO_2 exsolved from the TiO_2-rich glassy phase crystallizes initially as an unknown Ti–X phase which progressively decomposes at about 800° C into rutile. Subsequently, at higher temperatures, another amount of TiO_2 crystallizes at Li_2TiSiO_5. In any case no trace of TiO_2–anatase as well as of Li_2TiO_3 or $LiTiO_2$ was detected by us in all fibrous samples. Moreover, at about 950° C the rutile seemed to recrystallize into Li_2TiSiO_5 see Table II.

As for the phases containing aluminium, i.e. β-quartz (ss) and β-spodumene (ss) we noticed that their lattice parameters were very close to one another for every composition and at every temperature. Fig. 8 shows the values of a_0 and c_0 for the hexagonal β-quartz (ss) and for the tetragonal β-spodumene (ss) found in the present work (β-quartz (ss): $a_0 = 0.5020 \pm 0.0005$ nm and $c_0 = 0.5425 \pm 0.0005$ nm; β-spodumene (ss): $a_0 = 0.7459 \pm 0.0005$ nm and $c_0 = 0.8994 \pm 0.0005$ nm). These values agree with the plots reported by Nagakawa and Izumitani [20] and by Skinner and Evans [21] in which several solid solutions of various compositions for the β-quartz/β-eucryptite and β-spodumene/keatite systems were reported. In our case the β-quartz (ss) compositions are very close to pure β-quartz (~ 93 wt% of SiO_2), while in the case of β-spodumene (ss) an 88 wt% of SiO_2 can be computed.

All these results indicate that, in all probability, the 2nd exothermic DTA peak is due to two different causes: (a) phase transformation from β-quartz (ss) to β-spodumene (ss); (b) formation of the ternary phase Li_2TiSiO_5. On the other hand, the other two phases containing titanium, i.e. rutile and Ti–X, revealed by XRD at 800° C, did not give rise to any detectable heat effect by DTA.

The glass–ceramic materials obtained in bulk from glass IV, which do not contain aluminium, present a different crystallization path (see Table III). In this case the first exothermic effect was due to the formation of a lithium titanate phase (LT) whose XRD peaks agree better with the compound $LiTiO_2$ (cubic) than with the compound Li_2TiO_3 (monoclinic). Since the two strongest XRD peaks were superimposed in these two crystalline phases, it was not clear if both these phases were present or only the first one. After the 2nd DTA peak, at 820° C, α-quartz was present with hexagonal lattice constants equal to $a_0 = 0.4921 \pm 0.0003$ nm and $c_0 = 0.5403 \pm 0.0004$ nm very close to those reported in the

TABLE III Phase data of heat treated IV bulk sample

Heat treatment	Composition IV
680° C/2 h	LT(m)
720° C/2 h	M(m) D(s) LT(m)
820° C/2 h	D(m) M(m) R(vw) α-q(s) Ti–X(m)

Nomenclature:

LT = { Li_2TiO_3 (monoclinic); $LiTiO_2$ (cubic)

α-q = α-quartz,
D = Li-disilicate,
M = Li-metasilicate,
Ti–X = unknown phase.

literature [22]. By exclusion, this last result showed that the presence of aluminium favours the formation of β-quartz (ss) which subsequently changed into β-spodumene (ss) which was very rich in SiO_2.

3.3. Mechanical properties

Tensile strength and variation coefficients of the "as-quenched" fibres are reported in Table IV. It is possible to note that the fibres pertaining to the immiscibility dome (II and III) present a higher strength than the one shown by fibres I. In all cases these values were significantly higher than the value of the strength measured on E-glass fibres, under the same experimental conditions. The variation of the strength as a function of time at 700° C is reported in Fig. 9 for all three fibres examined, with time ranging between 5 and 15 min. Note the drastic fall of the strength within the first 5 min of heat treatment for each sample. Within the limits of error (see Table V) the trend is equal for all three fibres. Fig. 10 shows the early crystallization of fibres III as seen by SEM. Also the other two fibre samples show similar morphological features at the beginning of crystallization. Note that fibre I which was outside the immiscibility dome, presented

TABLE IV Tensile strength, confidence limits and variation coefficients for the "as-quenched" fibres I, II, III and for E-glass fibres

Composition	Tensile strength (MPa)	Confidence limits (95%)	Variation coefficients (%)
I	2107	± 78	15.4
II	2433	± 124	14.2
III	2261	± 103	14.0
E-glass fibres	1864	± 109	15.6

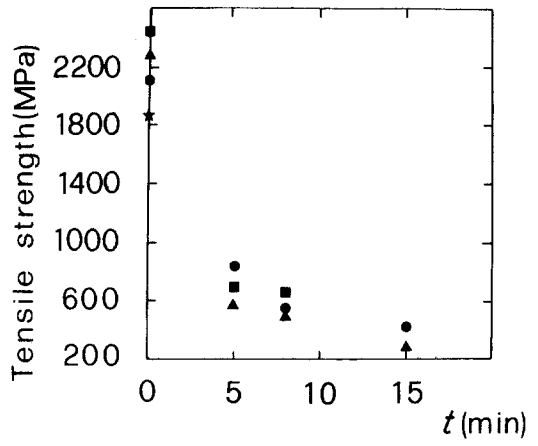

Figure 9 Plot of tensile strength against time for the three fibres heated at 700° C. (●) corresponds to fibre I; (■) corresponds to fibre II; (▲) corresponds to fibre III; (★) corresponds to fibre E.

after long times of crystallization, crystal preferred orientation which was not present in the other two heat-treated fibres II and III. Clearly, in the present study very short crystallization times were examined, and thus the differences in morphology and texture were not developed to an observable degree in relation to the mechanical behaviour.

The so-obtained values concerning the partially crystallized fibres were comparable with the results reported in the literature [1, 5]. The increase of the strength properties of the fibres after a controlled crystallization were observed by Wu *et al.* [1] on glass fibres having a very low initial strength (~ 300 MPa). On the contrary, in our case, we started with very high values of tensile strength (~ 2000 MPa), as can be seen in Table IV. Owing to their high fragility, it was not

TABLE V Confidence limits and variation coefficients for fibres I, II and III after different heat treatments at 700° C

Composition	Time	Confidence limits (95%)	Variation coefficients (%)
I	5 min	± 102	14.3
	8 min	± 87	27.6
	15 min	± 224	31.0
II	5 min	± 90	24.5
	8 min	± 82	23.0
III	5 min	± 75	24.7
	8 min	± 91	20.0
	15 min	± 121	33.3

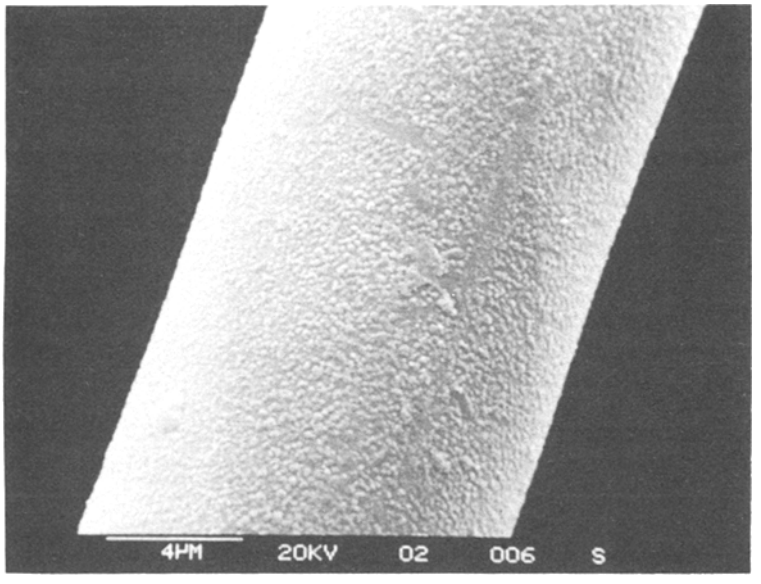

Figure 10 SEM micrograph on the early crystallization stage for fibre III.

possible to perform mechanical tests on fibres treated at temperatures corresponding to the 2nd exothermic peak.

4. Conclusions

The thermal evolution of the glass fibres of the system SiO_2–Li_2O–TiO_2–Al_2O_3 was extensively investigated by different techniques.

With regards to the formation of the compounds containing titanium we can suggest a crystallization mechanism similar to the one proposed by Furukawa and White [16] in the glass system Li_2O–$2SiO_2$–$0.3TiO_2$. A final ternary Li_2SiTiO_5 phase was always observed in all the fibres heated at high temperature ($> 850^\circ$ C). The role of aluminium was pointed out for what concerns the formation of β-quartz (ss) (1st DTA exothermic peak). The 2nd DTA exothermic peak was attributed to the β-quartz (ss) $\rightarrow$ β-spodumene (ss) phase transformation and to the crystallization of Li_2TiSiO_5.

Within the range of the compositions investigated here SEM and SAXS measurements on bulk materials have shown that a small addition of Al_2O_3 does not modify the limits of the immiscibility region present in the ternary system SiO_2–Li_2O–TiO_2. As to tensile strength, the "as-quenched" fibres of the composition placed within the immiscibility dome give higher values than those presented by the composition outside the liquid–liquid region. These values for the tensile strength are higher than those measured on E-glass fibres. A slight crystallization leads in all the fibres to a continuous decrease of the initial tensile strength. A tensile strength against time trend appears to be largely independent from the composition examined.

Acknowledgements

This work was supported by Italian C.N.R., "Progetto Finalizzato Chimica Fine e Secondaria – Sottoprogetto Metodologie".

We are indebted to Dr B. Locardi of Stazione Sperimentale del Vetro Murano (Venice) for furnishing the initial glasses and fibres.

Assistance in experimental work by Mr F. Venuda is gratefully acknowledged.

References

1. E. T. WU, T. YOSHIO and J. D. MACKENZIE, "Advances in Ceramics" Vol. IV, "Nucleation and Crystallization in Glasses," edited by J. H. S. Simons, I. R. Hulman and G. H. Beall (American Ceramic Society, Columbus, Ohio, 1982) p. 273.
2. B. LOCARDI, F. BARBON, A. ZAMBON and G. SORARÙ, *Rivista Sperim. Vetro* **12** (1982) 101.
3. A. BENEDETTI, G. FAGHERAZZI, S. MERIANI and G. SORARÙ, *J. Thermal Anal.* **29** (1984) 733.
4. J. F. BACON, *Appl. Polym. Symp.* **29** (1976) 117.
5. R. W. JONES and P. W. McMILLAN, *J. Non-Cryst. Solids* **38/39** (1980) 705.
6. A. BENEDETTI, G. COCCO, G. FAGHERAZZI, B. LOCARDI and S. MERIANI, *J. Mater. Sci.* **18** (1983) 1039.
7. A. BENEDETTI, G. COCCO, G. FAGHERAZZI, S. MERIANI and G. SCARINCI, *ibid.* **18** (1983) 1049.
8. S. MERIANI, G. FAGHERAZZI, B. LOCARDI and

G. SORARÙ, Thermal Analysis Vol. 1, Proceedings of the 7th International Conference in Thermal Analysis, edited by B. Miller (John Wiley, New York, 1982).
9. S. MERIANI, A. BENEDETTI, D. R. FESTA, B. LOCARDI, G. SCARINCI and G. SORARÙ, "Science of Ceramics", Vol. 12, edited by P. Vincenzini (Ceramurgica, Faenza, Italy, 1983) p. 419.
10. J. M. FIELDS Jr, W. D. LEAHY and J. BROWN JESSE Jr, Paper presented at the 72nd Annual American Ceramic Society Convention Philadelphia, Pennsylvania, 1970.
11. Phase Diagrams for Ceramists Fig. 474, E. Levin, C. R. Robbins and H. F. McMurdie (The American Ceramic Society, Columbus, Ohio, 1964) p. 172.
12. I. S. FEDOROVA and P. W. SCHMIDT, *J. Appl. Cryst.* **11** (1978) 405.
13. O. GLATTER, *ibid.* **13** (1980) 7.
14. C. G. GRANQVIST and R. A. BUHRMAN, *J. Catal.* **42** (1976) 477.
15. J. ZARZYCKY, *J. Appl. Cryst.* 7 (1974) 200.
16. T. FURUKAWA and W. B. WHITE, *Phys. Chem. Glasses* **20** (1979) 69.
17. K. NAKAGAWA and T. IZUMITANI, *ibid.* **10** (1969) 179.
18. M. AVRAMI, *J. Chem. Phys.* 7 (1939) 1103.
19. *Idem, ibid.* 8 (1939) 212.
20. K. NAKAGAWA and T. IZUMITANI, *J. Non-Cryst. Solids* 7 (1972) 168.
21. B. J. SKINNER and H. T. EVANS Jr, *Amer. J. Sci.* **258A** (1960) 312.
22. H. E. SWANSON and R. K. FUYAT, NBS Circular 539, Vol. III (1953) as reported in the JCPDS file* no. 5-0470.

Received 10 May
and accepted 31 July 1984